

Probing the Physical Properties of Directly Imaged Gas Giant Exoplanets Through Polarization

Mark S. Marley^{1*} and Sujan Sengupta^{2†}

¹*NASA Ames Research Center, MS-245-3, Moffett Field, CA 94035, U.S.A.*

²*Indian Institute of Astrophysics, Koramangala 2nd Block, Bangalore 560 034, India*

Submitted 2011 March 10.

ABSTRACT

It is becoming clear that the atmospheres of the young, self-luminous extrasolar giant planets imaged to date are dusty. Planets with dusty atmospheres may exhibit detectable amounts of linear polarization in the near-infrared, as has been observed from some field L dwarfs. The asymmetry required in the thermal radiation field to produce polarization may arise either from the rotation-induced oblateness or from surface inhomogeneities, such as partial cloudiness. While it is not possible at present to predict the extent to which atmospheric dynamics on a given planet may produce surface inhomogeneities substantial enough to produce net non-zero disk integrated polarization, the contribution of rotation-induced oblateness can be estimated. Using a self-consistent, spatially homogeneous atmospheric model and a multiple scattering polarization formalism for this class of exoplanets, we show that polarization on the order of 1% may arise due to the rotation-induced oblateness of the planets. The degree of polarization for cloudy planets should peak at the same wavelengths at which the planets are brightest in the near-infrared. The observed polarization may be even higher if surface inhomogeneities exist and play a significant role. Polarized radiation from self-luminous gas giant exoplanets, if detected, provides an additional tool to characterize these young planets and a new method to constrain their surface gravity and masses.

Key words: polarization – scattering – planets and satellites: atmospheres – stars:atmosphere.

1 INTRODUCTION

Several young, self-luminous gas giant planets have been detected by direct imaging (Chauvin et al. 2004; Marois et al. 2008, 2010; Lagrange et al. 2010; Lafrenière et al. 2010) around nearby stars. These objects are now being characterized by photometry and even spectroscopy (Bowler et al. 2010; Patience et al. 2010; Currie et al. 2011; Barman et al. 2011) in an attempt to characterize their atmospheres and constrain the planetary masses. In the next few years many more such planets are almost certainly to be detected by ground-based adaptive optics coronagraphs, such as the P1640 coronagraph on Palomar, the Gemini Planet Imager, and SPHERE on the VLT (Beichman et al. 2010).

The characterization of the mass of a given directly imaged planet can be problematical, since such planets typically lie at large star-planet separations (tens of AU and

greater) and are thus not amenable to detection by radial-velocity methods. Instead masses must be estimated either by comparison of photometry and spectroscopy to planetary evolutionary and atmospheric models or by their gravitational influence on other planets or disk (e.g. Kalas et al. 2005; Fabrycky & Murray-Clay 2010). Model comparisons as a method for constraining mass can be ambiguous, however. Evolution models which predict luminosity as a function of age have yet to be fully tested in this mass range for young planets and at very young ages (< 100 Myr) the model luminosity can depend on the unknown initial conditions (Marley et al. 2007; Fortney et al. 2008). The masses of the planets around HR 8799 estimated by cooling models are apparently inconsistent with standard model spectra (Bowler et al. 2010; Barman et al. 2011; Currie et al. 2011) and can lead to rapid orbital instabilities if circular, face-on orbits are assumed (Fabrycky & Murray-Clay 2010). Finally the mass of the planetary mass companion to the brown dwarf 2M1207 b (Chauvin et al. 2004) inferred from fitting of spectral models to observed near-infrared colors

* E-mail: Mark.S.Marley@NASA.gov

† E-mail: sujan@iiap.res.in

is discrepant with the mass inferred from the companion’s luminosity and the age of the primary (Mohanty et al. 2007).

Discrepancies such as these may arise because young exoplanets exist in a gravity-effective temperature (g, T_{eff}) regime in which both the evolutionary and atmospheric models have yet to be validated. Fits of photometry and spectroscopy to predictions of atmosphere models depend upon the veracity of the models themselves, which—in the T_{eff} range of interest—in turn sensitively depend upon model cloud profiles, which are as yet uncertain. Extensive experience with fitting models to brown dwarf spectra and photometry (Cushing et al. 2008; Stephens et al. 2009) reveals that while effective temperature can be fairly tightly constrained, gravity determinations are usually less precise, uncertain in some cases by almost an order of magnitude in g . While there are low gravity spectral indicators recognized from surveys of young objects (Cruz et al. 2009; Kirkpatrick et al. 2006) these have yet to be calibrated by studies of binary objects which allow independent measures of mass. Ideally for a single object with a given radius R , evolution model luminosity, which (for a known parallax) constrains $R^2 T_{\text{eff}}^4$ would be fully consistent with (g, T_{eff}) constraints from atmosphere model fitting. But, as noted above, this is often not in fact the case, as the derived luminosity, mass, and radii of the companion to 2M1207 b as well as the HR 8799 planets are not fully internally self-consistent with standard evolution models.

Given the likely future ubiquity of direct detections of young, hot Jupiters and the clear need for additional independent methods to constrain planet properties, we have explored the utility of polarization as an additional method for characterizing self-luminous planets.

Polarization of close-in giant exoplanets whose hot atmosphere favours the presence of silicate condensates, is discussed by Seager, Whitney & Sasselov (2000) and by Sengupta & Maiti (2006). While these authors considered the polarization of the combined light from an unresolved system of star and planet, Stam, Hovenier & Waters (2004) presented the polarization of the reflected light of a resolved, directly-imaged Jupiter-like exoplanet. Since the polarized light of a close-in exoplanet is combined with the unpolarized continuum flux of the star which cannot be resolved, the amount of observable polarization in such case is extremely low – of the order of magnitude of planet-to-star flux ratio. Polarization measurements of directly-imaged exoplanets in reflected light is also challenging. The removal of scattered light from the primary star must be precise in both polarization channels so that the planet’s intrinsic polarization (which is a differential measurement) can be accurately determined. In any case no extrasolar planet has yet been imaged in scattered light, an accomplishment that will likely require a space-based coronagraph (e.g., Boccaletti et al. 2011). Measuring polarization of thermally emitted radiation—as we propose here—is also difficult but does not require a planet to be close to the star (where the starlight suppression is most difficult) so that it is bright in reflected light. Furthermore extrasolar planets have already been imaged which raises the possibility of polarization observations.

It is clear from comparisons of model spectra to data that most of the exoplanets directly imaged to date have dusty atmospheres (Marois et al. 2008; Bowler et al. 2010;

Lafrenière et al. 2010; Barman et al. 2011; Currie et al. 2011; Skemer et al. 2011). Clear atmospheres lacking dust grains can be polarized, but only at blue optical wavelengths where gaseous Rayleigh scattering is important (Sengupta & Marley 2009). Since even the hottest young exoplanets will not emit significantly in the blue, grain scattering must be present for there to be measurable polarization in the near-infrared where warm giant planets are bright (Sengupta & Marley 2010). There are two temperature ranges within which we expect a gas giant exoplanet to possess significant atmospheric condensates. The first is L-dwarf like planets (roughly $1000 < T_{\text{eff}} < 2400$ K) where iron and silicate grains condense in the observable atmosphere. The lower end of this range in the planetary mass regime is as yet uncertain. The second temperature range occurs in cool planets with atmospheric water clouds ($T_{\text{eff}} < 400$ K). There have yet been no confirmed detections of such planets. Here we will focus on the first category since such objects are brighter, more easily detectable, and the comparison to the field dwarfs is possible.

Although survey sizes are fairly small, linear polarization of field L dwarfs has been detected. Menard et al. (2002) and Zapatero Osorio et al. (2005) both report that a fraction of L dwarfs, particularly the later, dustier spectral types, are intrinsically polarized. Sengupta & Marley (2010) find that the observed polarization can plausibly arise from emission of cloudy, oblate dwarfs, although to produce the required oblateness (20% or more) the dwarfs must have fairly low gravity for a field dwarf ($g \sim 300 \text{ m s}^{-2}$) and rapid rotation. The required rotation periods are brisk, as little as 2 hours or less, but are compatible with observed rotational velocities in at least some cases (see Sengupta & Marley (2010) for a discussion). Sengupta & Marley (2010) further find that the near-infrared polarization is greatest at $T_{\text{eff}} \sim 1600$ K where their model condensate clouds are both optically thick and still prominent enough in the photosphere to maximally affect the polarization.

Surface inhomogeneities can also give rise to a net polarization (Menard & Delfosse 2004) and experience from the solar system confirms that irregularly spaced clouds are to be expected. Both Jupiter’s and Saturn’s thermal emission in the five-micron spectral window is strongly modulated by horizontally inhomogeneous cloud cover and it would not be surprising to find similar morphology in the atmospheres of exoplanets. In the presence of surface inhomogeneity, the asymmetry that produces the net non-zero disk-integrated polarization would increase and hence a combination of oblate photosphere and surface inhomogeneity can give rise to detectable levels of polarization.

Exoplanets are even better candidates than L dwarfs to have an oblate shape and be polarized. With a lower mass and roughly the same radius as a brown dwarf (and thus a lower gravity), a rapidly rotating planet can be significantly oblate and consequently produce a polarization signal even without surface inhomogeneities. Here we explore the conditions under which the thermal emission from a warm, young exoplanet may be polarized and consider the scientific value of measuring exoplanet polarization. We first look at the issue of oblateness, then present a set of cloudy model atmosphere calculations relevant to planets amenable to direct detection and discuss under which conditions their thermal emission may be polarized. Finally we discuss our findings

and explore how the characterization of an extrasolar planet may be enhanced by polarization observations.

2 YOUNG GIANT EXOPLANETS

2.1 Evolution

When giant planets are young they are thermally expanded and boast larger radii and smaller gravity. Fortney et al. (2008) have computed evolution models for gas giant planets with masses ranging from 1 to 10 M_J for ages exceeding 10^6 yr and we can use their results to predict the oblateness of thermally expanded young Jupiters with various rotation rates. Those authors modeled two types of evolution models. The first variety, termed ‘hot starts’, was most traditional and assumed the planets formed from hot, distended envelopes of gas which rapidly collapsed. This calculation is comparable to that of most other workers in the field. They also presented calculations for planets formed by the core accretion planet formation process (see Lissauer & Stevenson (2007)) which (depending on details of the assumed boundary condition for the accretion shock) produces planets that are initially much smaller and cooler than in the ‘hot start’ scenario.

For the calculations here we choose to use the ‘hot start’ evolutionary calculation. We do this for several reasons. First, these models provide a reasonable upper limit to the radius at young ages and thus bound the problem. Second, at the large orbital separations that will, at least initially, be probed by ground based adaptive optics coronagraphic imaging, the core accretion mechanism may be inefficient at forming planets. Thus the gaseous collapse scenario may be more relevant choice. Finally the three planets observed around HR 8799 are all much brighter than predicted by the Fortney et al. (2008) cold-start, but not the hot-start, cooling tracks.

Figure 1 presents model evolution tracks for non-irradiated giant exoplanets from Fortney et al. (2008). On this figure planets age from the right to the left as effective temperature falls, the planets contract, and their surface gravity, g , increases. The dashed lines denote isochrones. This figure guides our selection of atmosphere models to evaluate for polarization studies. Groundbased coronagraphic searches for planets are expected to focus on stars younger than about 200 Myr (e.g., McBride et al. 2011). From the figure we see that at ages of 10 to 200 Myr we expect exoplanets with masses falling between 1 and 10 M_J to have g roughly in the range of 15 to 200 m s^{-2} .

2.2 Shape

Both Jupiter and Saturn are oblate. The fractional difference, $f = 1 - R_p/R_e$, between their equatorial and polar radii, known as oblateness, are 0.065 and 0.11 respectively. The extent to which their equators bulge outwards depends on their surface gravity, g , and rotation rate, Ω , as well as their internal distribution of mass. The Darwin-Radau relationship (Barnes & Fortney 2003) connects these quantities of interest:

$$f = \frac{\Omega^2 R_e}{g} \left[\frac{5}{2} \left(1 - \frac{3K}{2} \right)^2 + \frac{2}{5} \right]^{-1} \quad (1)$$

Here $K = I/(MR_e^2)$, I is the moment of inertia of the spherical configuration, and M and R_e are the mass and equatorial radii.

The relationship for the oblateness f of a stable polytropic gas configuration under hydrostatic equilibrium is also derived by Chandrasekhar (1933) and can be written as

$$f = \frac{2}{3} C \frac{\Omega^2 R_e}{g} \quad (2)$$

where C is a constant whose value depends on the polytropic index.

The above two relationships provide the same value of oblateness for any polytropic configuration. Equating Eq. (1) and Eq. (2), we obtain

$$C = \frac{3}{2} \left[\frac{5}{2} \left(1 - \frac{3K}{2} \right)^2 + \frac{2}{5} \right]. \quad (3)$$

Substituting the value of K for a polytrope of index n gives the value of the corresponding C . For example, $K = 0.4, 0.261, 0.205, 0.155, 0.0754$ for $n = 0, 1, 1.5, 2, 3$ respectively. The corresponding values of C derived by Chandrasekhar (1933)(p. 553, Table 1). are 1.875, 1,1399, 0.9669, 0.8612, 0.7716 respectively.

The interiors of gas giant planets can be well approximated as $n = 1$ polytropes. For the observed mass, equatorial radii, and rotation rates of Jupiter and Saturn, expression (2) predicts, with $n = 1$, an oblateness of 0.064 and 0.11, in excellent agreement with the observed values. Figure 2 presents the oblateness computed employing Eq. (2) as applied to 1 and 10 M_J planets at three different ages, 10, 100, and 1,000 Myr using the Fortney et al. (2008) hot-start cooling tracks. Also shown is the oblateness (0.44) at which a uniformly rotating $n = 1.0$ polytrope becomes unstable (James 1964). Clearly for rotation rates comparable to those seen among solar system planets we can expect a substantial degree ($f > 0.10$) of rotational flattening. As gas giants age and contract the same rotation rate produces much less oblate planets. However for young, Jupiter mass planets rotation rates of 7 to 10 hours can easily produce $f \sim 0.2$ even for planets as old as 100 Myr. More rapid rotation rates may produce even greater degrees of flattening. L dwarfs, with much higher surface gravity, must have even more rapid rotation rates to exhibit even modest flattening (Sengupta & Marley 2010).

3 POLARIZATION OF YOUNG EXOPLANETS

To explore the degree of polarization expected for various planet masses and ages we considered a selection of one-dimensional, plane-parallel, hydrostatic, non-gray, radiative-convective equilibrium atmosphere models with sixty vertical layers (Ackerman & Marley 2001; Marley et al. 2002; Freedman et al. 2008) for specified effective temperatures, $800 < T_{\text{eff}} < 1200$ K and surface gravities $g = 30$ and 100 m sec^{-2} . We focus on this apparently limited parameter range since all gas giant exoplanets with masses below 10 M_J will have cooled below 1200 K by an age of 30 Myr (see Figure 1 and also Fortney et al. (2008)). The median age for nearby (< 75 pc) young stars that are likely targets for planet imaging surveys is 50 Myr (McBride et al. 2011). For

our study we choose a lower limit of 800 K, well below the T_{eff} at which Sengupta & Marley (2010) predicted maximal polarization for field L dwarfs. At such temperatures dust clouds, if present globally across the disk, will lie at high optical depth and we expect produce a smaller polarization signal than the warmer objects.

Indeed 800 K is well below the field dwarf L to T transition temperature of 1200 to 1400 K (Stephens et al. (2009) and references therein) by which point most signs of clouds have departed. However there exists growing evidence that there is a gravity dependence to the effective temperature at which clouds are lost from the atmosphere and certainly the planets such as those orbiting HR 8799 are still dusty at effective temperatures near 1000 K (Bowler et al. 2010). Observation of a polarization signal in a cooler exoplanet would provide powerful evidence for atmospheric dust.

Some of the more massive young exoplanets ($M > 8 M_{\text{J}}$) may have gravities in excess of our 100 m sec^{-2} upper limit, but as we show below little oblateness-induced polarization is expected at high gravity in this T_{eff} range (see also Sengupta & Marley (2010)). For example a surface gravity of $g = 100 \text{ m sec}^{-2}$ and $T_{\text{eff}} = 1000 \text{ K}$ approximately describes an $8 M_{\text{J}}$ planet at an age of 100 Myr while values of 30 m sec^{-2} and 800 K are expected for a $2 M_{\text{J}}$ planet at an age of 60 Myr. We choose these values and a few others to illustrate the parameter space and the sensitivity of the results to variations in gravity and effective temperature.

Each model includes atmospheric silicate and iron clouds computed with sedimentation efficiency (Ackerman & Marley 2001) $f_{\text{sed}} = 2$. Preliminary studies by our group suggest that even dustier models with $f_{\text{sed}} \sim 1$ might be necessary to reproduce the HR 8799 planets. However our previous work (Sengupta & Marley 2010) has demonstrated that while $f_{\text{sed}} = 1$ atmospheres do show greater polarization than $f_{\text{sed}} = 2$, the difference is slight when integrated over the disk. Other cloud modeling approaches are reviewed by Helling et al. (2008). Some of these alternative cloud modeling formulations, such as those employed by Helling and collaborators (e.g., Helling & Woitke 2006; Helling et al. 2008), predict a greater abundance of small particles high in the atmosphere than the Ackerman & Marley approach. Such a haze of small particles could potentially produce a larger polarization signal than we derive here. Polarization measurements may thus help provide insight into the veracity of various approaches.

As in Sengupta & Marley (2010) we employ the gas and dust opacity, the temperature-pressure profile and the dust scattering asymmetry function averaged over each atmospheric pressure level derived by the atmosphere code in a multiple scattering polarization code that solves the radiative transfer equations in vector form to calculate the two Stokes parameter I and Q in a locally plane-parallel medium (Sengupta & Marley 2009). For each model layer we fit a Henyey-Greenstein phase function to the particle scattering phase curve predicted by a Mie scattering calculation. A combined Henyey-Greenstein-Rayleigh phase matrix (Liu & Weng 2006) is then used to calculate the angular distribution of the photons before and after scattering. In the near-infrared the contribution of Rayleigh scattering by the gas to the overall scattering is negligible and the scattering is treated in the Henyey-Greenstein limit with the particle phase function computed from Mie theory. Specifi-

cally the off diagonal terms of the scattering phase matrix are described by White (1979) and are very similar to the pure Rayleigh case. For the diagonal elements the Henyey-Greenstein elements are used. In the limit of the scattering asymmetry parameter approaching zero the matrix converges to the Rayleigh scattering limit. Finally, the angle dependent I and Q are integrated over the rotation-induced oblate disk of the object by using a spherical harmonic expansion method and the degree of polarization is taken as the ratio of the disk integrated polarized flux (F_Q) to the disk integrated total flux (F_I). The detailed formalisms as well as the numerical methods are provided in Sengupta & Marley (2009).

Figures 3 and 4 illustrate typical input properties of the models employed here. Figure 3 shows a model temperature-pressure profile along with iron and silicate condensate grain sizes as computed by our cloud model. Figure 4 shows the mean layer single scattering albedo, $\overline{\omega_0}$, and scattering asymmetry parameter, $\cos \theta$, as a function of wavelength near the peak opacity of the cloud. Within strong molecular bands the single scattering albedo approaches zero since gas absorption dominates over the cloud opacity. Below the cloud base and far above the cloud both the albedo and asymmetry parameters are essentially zero in the near infrared as gaseous Rayleigh scattering makes little contribution to the opacity at those wavelengths. Note that for the computed particle sizes the cloud is strongly forward scattering at wavelengths where cloud opacity dominates molecular absorption in agreement with a recent study by de Kok et al. (2011).

4 RESULTS AND DISCUSSIONS

Figure 5 presents the computed thermal emission and polarization spectra of an approximately 10 Myr old 2 Jupiter mass planet assuming rotation periods of 5 and 6 hrs. The striking dependence of polarization on the rotation rate arises from the sensitivity of oblateness to rotation period as seen in Figure 2. Generally speaking the degree of polarization is highest at those wavelengths of low gaseous opacity where the cloud is visible while at other wavelengths, inside of atomic and molecular absorption bands, flux emerges from higher in the atmosphere and is less influenced by cloud scattering. While the degree of polarization peaks at the shortest wavelengths shown (from the influence of gaseous Rayleigh scattering), there is very little flux at optical wavelengths. However in the near-infrared, where windows in the molecular opacity allow flux to emerge from within the clouds, the computed degree of polarization approaches 1%. In these spectral regions the planets will be bright, the contrast with the primary star favorable, and thus the polarization may be more easily detectable at this level. Beyond about $2.2 \mu\text{m}$ thermal emission emerges from above the cloud tops and thus there is no signature of the scattering and the net polarization is near zero. This pattern of polarization is diagnostic of atmospheric clouds and is easily distinguished from other sources of polarization, for example a circumplanetary disk.

Figures 6 and 7 show warmer model cases for the same gravity with similar behavior. These cases would apply to quite young planets at an age of less than ten million years,

but illustrate that the degree of polarization does not dramatically increase at higher effective temperatures. Figure 8 shows the variation with gravity. With a fixed rotation period of five hours, models with g of 56 and 100 m s^{-2} show very little polarization at any wavelength. These models would correspond to approximately 4 to 6 Jupiter mass planets at ages greater than 10 million years, perhaps typical of the planet types that may be directly imaged. The sensitivity of polarization to gravity seen in this figure illustrates the promise of polarization, in the right circumstances, to provide a new constraint on exoplanet mass.

Figure 9 generalizes these trends, showing the predicted polarization in I and J bands as a function of the rotational period P_{rot} . For a fixed surface gravity and viewing angle, i , the degree of polarization does not vary substantially within the range of T_{eff} between 800 and 1200 K. The polarization profiles in both bands increase with decreasing rotation period and the polarization is generally greater in J than in I band. As is the case for brown dwarfs (Sengupta & Marley 2010), for a given rotation period the polarization decreases with lower i .

All of the cases shown in Figure 9 have an oblateness less than 0.44, the stability limit for an $n = 1$ polytrope. For $g = 30 \text{ m s}^{-2}$ the stability limit is reached at a rotation period of about 4 hours, slightly less than the lower limit shown on the figure. Such short rotation periods may in fact be a natural consequence of giant planet formation in a circumstellar binary as the angular momentum of accreting gas naturally produces rapid rotation rates (Ward & Canup 2010).

We conclude that a self-luminous gas giant planet—even with a homogeneous cloud distribution—will exhibit notable polarization (greater than a few tenths of percent) in the near infrared if the planet is (1) cloudy, (2) significantly oblate, and (3) viewed at a favorable geometry. An oblate shape is the easiest to obtain at low masses and modest rotation rates or higher masses and more rapid rotation rates. Higher effective temperatures, which would produce more dust higher in the atmosphere and more polarization (Sengupta & Marley 2010), are generally excluded by the evolution for ages greater than a few million years. More massive planets, which take longer to cool, have higher gravity and thus a smaller oblateness and less polarization (Figures 2 & 9) for a given rotation rate. Given these considerations we believe the cases we have presented here are among the more favorable for homogenous cloud cover. While we have not considered every combination of parameters, the models presented here along with perturbations of those models we have also studied lead us to conclude that uniformly cloudy planets will not present polarization greater than a few percent and polarization is most likely to be found for young, low mass, rapidly rotating planets.

However inhomogeneous cloud cover, which we have not modeled, may also affect the polarization spectra. Indeed an inhomogeneous distribution of atmospheric dust (e.g., Jupiter-like banding) would not be unexpected. Such banding may provide further asymmetry (Menard & Delfosse 2004) and hence increase (or even decrease) the net non-zero polarization. A non-uniform cloud distribution may be the mechanism that underlies the L to T-type transition among brown dwarfs (Ackerman & Marley 2001; Burgasser et al. 2002; Marley et al. 2010) and variability has been detected in

some transition dwarfs (Artigau et al. 2009; Radigan et al. 2011). Cloud patchiness is also observed in images of thermal emission from Jupiter and Saturn taken in the M-band (five-micron) spectral region (e.g. Westphal 1969; Westphal et al. 1974; Orton et al. 1996; Baines et al. 2005), so patchiness may indeed be common. Polarization arising from patchy clouds still requires the presence of some clouds of course, thus any polarization detection provides information on the presence of condensates and—by extension—constrains the atmospheric temperature.

5 CONCLUSIONS

The next decade is expected to witness the discovery of a great many self-luminous extrasolar giant planets (Beichman et al. 2010). The masses, atmospheric composition and thermal structure of these planets will be characterized by photometry and spectroscopy. For some systems, other constraints, such as dynamical interactions with dust disks or potential instabilities arising from mutual gravitational interactions (e.g., Fabrycky & Murray-Clay 2010) may also contribute. Here we demonstrate that measurable linear polarization in I or J bands reveals the presence of atmospheric condensates, thereby placing limits on atmospheric composition and temperature. Polarization of thermal emission from a homogeneously cloudy planet is most favored for young, low mass, and rapidly rotating planets. A diagnostic characteristic of cloud-induced polarization is that the polarization peaks in the same spectral bandpasses as the flux from the planet because photons are emerging from within the cloud itself as opposed to higher in the atmosphere (Figures 5 through 8).

Assuming that our atmospheric and condensate cloud models are reasonably accurate, we conclude that any measured polarization greater than about 1% likely can be attributed to inhomogeneities in the global cloud deck. While we have not considered every possible model case, we find that our most favorable plausible cases do not produce notably greater polarization. Other cloud models (e.g., Helling & Woitke 2006; Helling et al. 2008) which incorporate more small particles high in the atmosphere may well produce a different result, thus polarization may help to distinguish such cases. For a fixed rotation period, the oblateness and thus polarization increases with decreasing surface gravity. In such situations polarization may provide a new constraint on gravity and mass. However for gravity in excess of about 50 m s^{-2} and for $T_{eff} < 1200 \text{ K}$ (corresponding to planet masses greater than about $4 M_J$) we do not expect detectable amounts of polarization. Warmer and higher gravity field L dwarfs, can show measurable polarization since such cloud decks are higher in the atmosphere. For directly imaged exoplanets, however, we do not expect to encounter such high effective temperatures. For exoplanets with plausible $T_{eff} < 1200 \text{ K}$, Figure 9 shows that even if the rotation period is as rapid as 4.5 hrs. and the viewing angle is 90° at which the polarization is maximum, the percentage degree of polarization in thermal emission is not more than a few times of 10^{-2} .

The aim of our study was to better understand the information conveyed by polarization about the properties of extrasolar giant planets directly imaged in their thermal

emission. We have found that in some cases polarization can provide additional constraints on planet mass, atmospheric structure and cloudiness. Combined with other constraints, polarization adds to our understanding, although there remain ambiguities. A study of the polarization signature of partly cloudy planets would yield further insight into the value of polarization measurements for constraining extrasolar giant planet properties.

6 ACKNOWLEDGEMENTS

We thank the anonymous referee for helpful comments that improved the manuscript. MSM recognizes the NASA Planetary Atmospheres Program for support of this work.

REFERENCES

- Ackerman, A. & Marley, M. S. 2001, *ApJ*, 556, 872.
- Artigau, É., Bouchar, S., Doyon, R., & Lafrenière, D. 2009, *ApJ*, 701, 1534
- Baines, K. H., et al. 2005, *Earth Moon and Planets*, 96, 119
- Barman, T. S., Macintosh, B., Konopacky, Q. M., & Marois, C. 2011, *Ap.J.*, 733, 65
- Barnes, J. W. & Fortney, J. J. 2003, *ApJ*, 588, 545.
- Beichman, C. A., et al. 2010, *Proc. Astron. Soc. Pac.*, 122, 162
- Boccaletti, A., et al. 2011, *Experimental Astronomy*, in press.
- Bowler, B. P., Liu, M. C., Dupuy, T. J., & Cushing, M. C. 2010, arXiv:1008.4582
- Burgasser, A. J., Marley, M. S., Ackerman, A. S., Saumon, D., Lodders, K., Dahn, C. C., Harris, H. C., & Kirkpatrick, J. D. 2002, *Ap.J.Lett.*, 571, L151
- Chandrasekhar, S. 1933, *MNRAS*, 93, 539
- Chauvin, G., Lagrange, A.-M., Dumas, C., Zuckerman, B., Mouillet, D., Song, I., Beuzit, J.-L., & Lowrance, P. 2004, *Aston. Astoph.*, 425, L29
- Cruz, K. L., Kirkpatrick, J. D. & Burgasser, A. J. 2009, *A.J.*, 137, 3345.
- Currie, T., et al. 2011, *Ap J.*, 729, 128
- Cushing, M. C. et al. 2008, *ApJ*, 678,1372.
- de Kok, R., Helling, Ch., Stam, D., Woitke, P., & Witte, S. 2011, arXiv:1105.3062
- Fabrycky, D. C. & Murray-Clay, R. A. 2010, *Ap.J.*, 710, 1408.
- Fortney, J. J., Marley, M. S., Saumon, D., & Lodders, K. 2008, *Ap.J.*, 683, 1104
- Freedman, R. S. et al. 2008, *ApJS*, 174, 71.
- Helling, C., et al. 2008, *MNRAS*, 391, 1854
- Helling, C., & Woitke, P. 2006, *A&Ap.*, 455, 325
- Helling, C., Dehn, M., Woitke, P., & Hauschildt, P. H. 2008, *Ap.J.Let.*, 675, L105
- James, R. 1964, *ApJ*, 140, 552
- Kalas, P., Graham, J. R., & Clampin, M. 2005, *Nature*, 435, 1067
- Kirkpatrick, J. D. et al. 2006, *ApJ*, 639, 1120.
- Lafrenière, D., Jayawardhana, R., & van Kerkwijk, M. H. 2010, *Ap.J.*, 719, 497
- Lagrange, A.-M., et al. 2010, *Science*, 329, 57
- Lissauer, J. J., & Stevenson, D. J. 2007, *Protostars and Planets V*, 591
- Liu,Q. & Weng, F. 2006, *Applied Optics*, 45, 7475.
- Marley, M. S. et al. 2002, *ApJ*, 568, 335.
- Marley, M. S., Fortney, J. J., Hubickyj, O., Bodenheimer, P., & Lissauer, J. J. 2007, *Ap.J.*, 655, 541
- Marley, M. S., Saumon, D., & Goldblatt, C. 2010, *Ap.J.Lett.*, 723, L117
- Marois, C., Macintosh, B., Barman, T., Zuckerman, B., Song, I., Patience, J., Lafreniere, D., & Doyon, R. 2008, *Science*, 322, 5906
- Marois, C., Zuckerman, B., Konopacky, Q. M., Macintosh, B., & Barman, T. 2010, *Nature*, 468, 1080
- McBride, J., Graham, J., Macintosh, B., Beckwith, S., Marois, C., Poyneer, L., Wiktorowicz, S. 2011, arXiv:1103.6085
- Ménard, F. et al. 2002, *A&A*, 396, L35.
- Menard, F. & Delfosse, X. 2004, *Semaine de l’Astrophysique Francaise*, ed. F. Combes et al. (EDP-Sciences : Paris 2004) 305.
- Mohanty, S., Jayawardhana, R., Huélamo, N., & Mamajek, E. 2007, *ApJ*, 657, 1064
- Orton, G., et al. 1996, *Science*, 272, 839
- Patience, J., King, R. R., de Rosa, R. J., & Marois, C. 2010, *A&A*, 517, A76
- Radigan, J., et al. 2011, *ApJ* in prep
- Seager, S., Whitney, B. A., & Sasselov, D. D. 2000, *ApJ*, 540, 504
- Sengupta, S. & Maiti, M. 2006, *ApJ*, 639, 1147
- Sengupta, S. & Marley, M. S. 2009, *ApJ*, 707, 716
- Sengupta, S. & Marley, M. S. 2010, *ApJL*, 722, L142
- Skemer, A. J., Close, L. M., Szűcs, L., Apai, D., Pascucci, I., & Biller, B. A. 2011, *ApJ*, 732, 107
- Stam, D. M., Hovenier, J. W., & Waters L. B. F. M. 2004, *A & A*, 428, 663
- Stephens, D. C. et al. 2009, *ApJ*,702,154.
- Ward, W. R., & Canup, R. M. 2010, *Astron. J.*, 140, 1168
- Westphal, J. A. 1969, *Ap.J.L.*, 157, L63
- Westphal, J. A., Matthews, K., & Terrile, R. J. 1974, *Ap.J.L.*, 188, L111
- White, R. L. 1979, *ApJ*, 229, 954
- Zapatero Osorio, M. R. et al. 2005, *ApJ*, 621, 445.

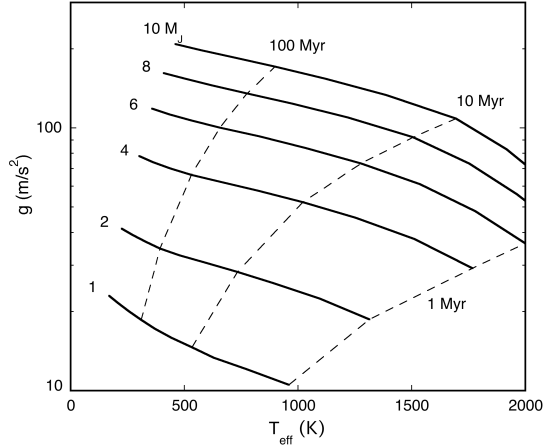


Figure 1. Evolution through time in $T_{\text{eff}} - g$ space of non-irradiated, metallicity $[M/H] = 0.0$ giant planets of various masses. Solid lines are evolution tracks at various fixed masses ranging from 1 to $10 M_J$. Dashed lines are isochrones for various fixed ages since an arbitrary ‘hot start’ initial model (Fortney et al. 2008).

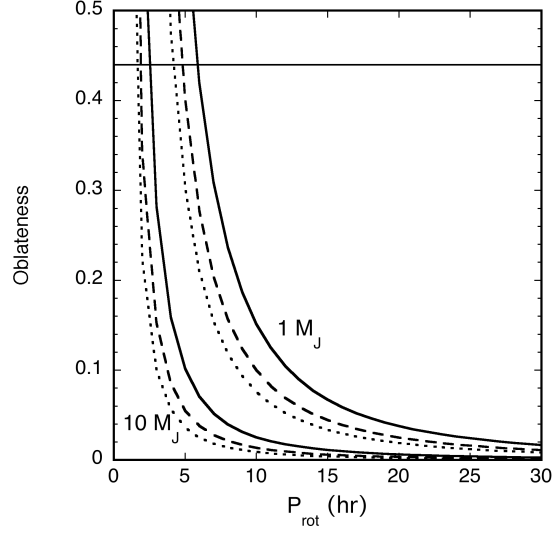


Figure 2. Rotationally induced oblateness as a function of rotational period for 1 and $10 M_J$ planets with three different ages (10 - solid, 100 - dashed, and 1000 Myr - dotted). Horizontal line is the stability limit for $n = 1$ polytropes assuming solid body rotation. More rapidly rotating planets would form a triaxial ellipsoidal shape and eventually bifurcate.

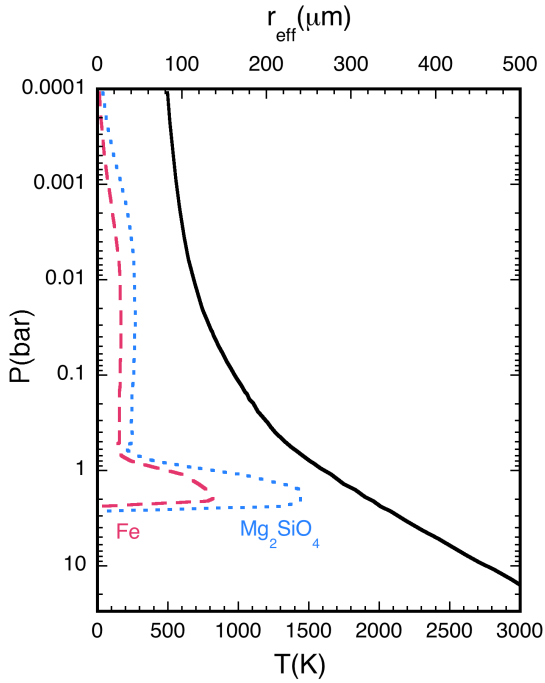


Figure 3. Atmospheric temperature (T , lower scale) and cloud particle size, r_{eff} , (upper scale) as a function of pressure, P , for one adopted model atmosphere with $T_{\text{eff}} = 1000 \text{ K}$, $g = 30 \text{ m s}^{-2}$, and $f_{\text{sed}} = 2$. From Figure 2 this corresponds to approximately a $2.5 M_{\text{J}}$ planet at an age of a few million years. Particle sizes are shown for iron and silicate (forsterite) grains, the two most significant contributors to cloud opacity. Shown is the “effective radius” (r_{eff}) of the particles, a mean size precisely defined in Ackerman & Marley (2001).

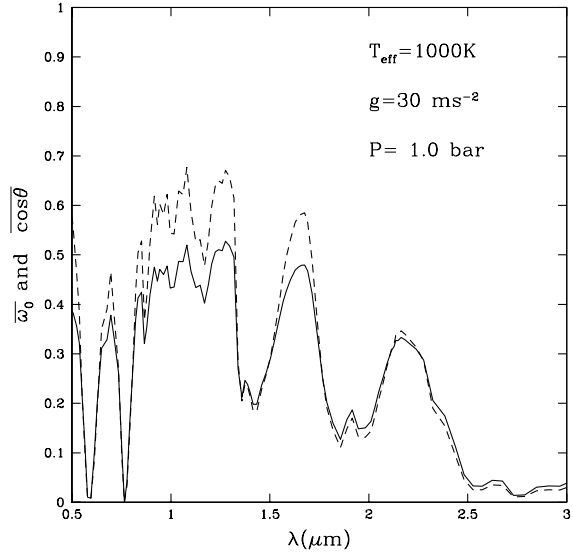


Figure 4. Scattering properties as a function of wavelength, λ , of a model layer near the 1 bar pressure level for the model atmosphere shown in Figure 3. Shown are the layer single scattering albedo, $\overline{\omega_0}$, solid, and the layer asymmetry parameter, $\overline{\cos \theta}$, dashed. In strong molecular bands gaseous absorption dominates over scattering, thus lowering the mean layer albedo.

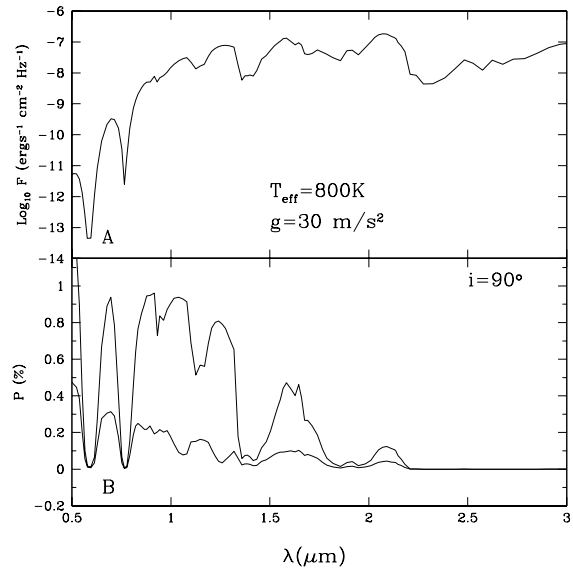


Figure 5. The emergent flux (A) and the disk-integrated degree of linear polarization $P(\%)$ (B) of non-irradiated exoplanets at different wavelengths at viewing angle $i = 90^\circ$ (equatorial view). In (B), the top solid line represents the polarization profile for a rotational period $P_{\text{rot}} = 5 \text{ hr}$ while the bottom solid line represents that for 6 hr . Note that while the polarization can be high at blue wavelengths there is very little flux there.

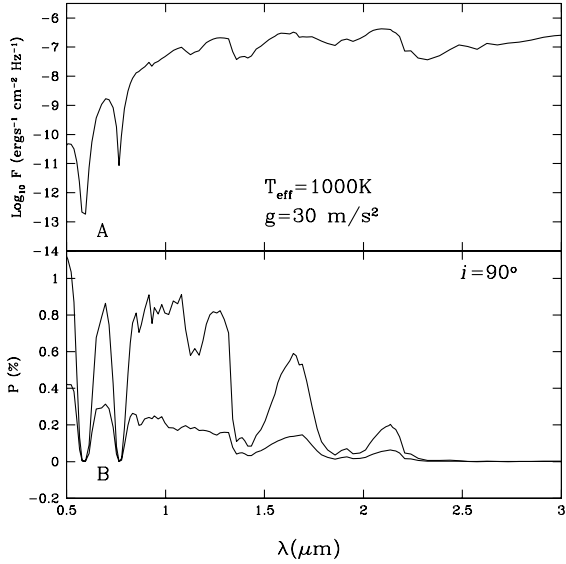


Figure 6. Same as figure 5 but with $T_{\text{eff}} = 1000\text{K}$. This is the result for the model characterized in Figures 3 and 4.

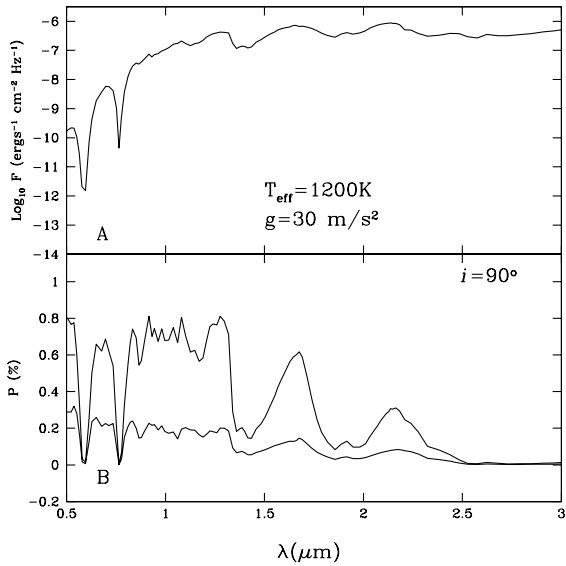


Figure 7. Same as figure 5 but with $T_{\text{eff}} = 1200\text{K}$.

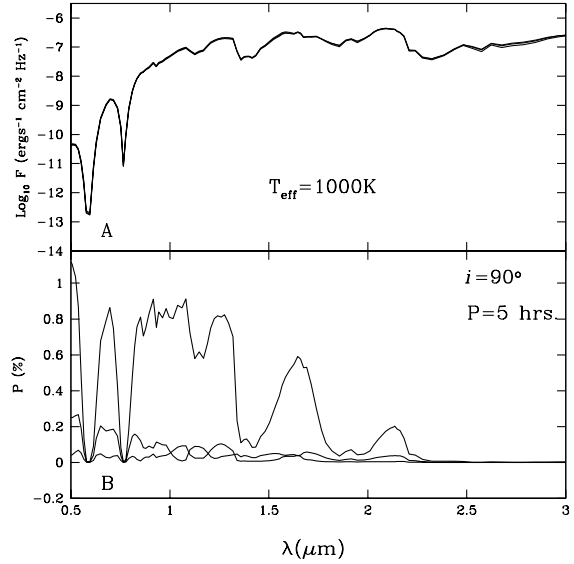


Figure 8. The emergent flux (A) and the disk-integrated degree of linear polarization (B) of non-irradiated exoplanets for a fixed $T_{\text{eff}} = 1000\text{K}$ but for different surface gravities. In (B), the solid lines from top to bottom represent the polarization profiles for surface gravity $g = 30, 56$ and 100 m s^{-2} respectively. The difference in the emergent flux (A) for a fixed effective temperature but surface gravity varying over this range is not noticeable on this scale.

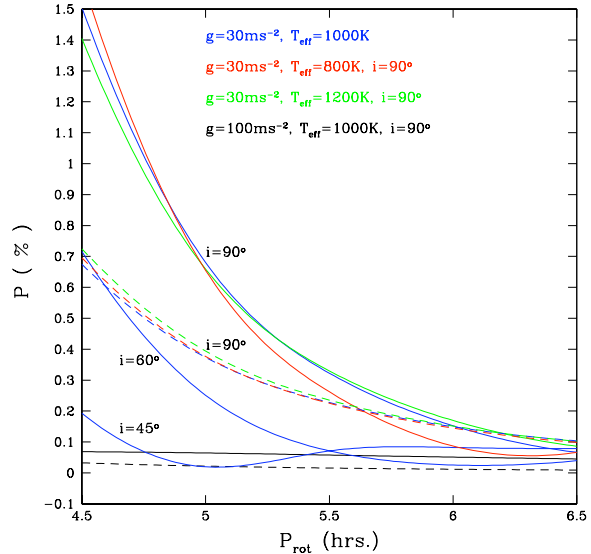


Figure 9. Scattering polarization profiles of non-irradiated exoplanets with different rotational periods. The solid lines represent the percentage degree of linear polarization in J-band while the broken lines represent that in I-band. A variety of model cases are shown, all assume $f_{\text{sed}} = 2$. Cases are shown for viewing angle $i = 90^\circ$ (equator view) and $i = 60$ and 45° .